Rotating and static sources for gamma knife radiosurgery systems: Monte Carlo studies

J. Y. C. Cheung and K. N. Yu[a)]
Department of Physics and Materials Science, City University of Hong Kong, Kowloon Tong, Kowloon, Hong Kong

(Received 1 February 2006; revised 8 April 2006; accepted for publication 29 April 2006; published 21 June 2006)

Rotating gamma systems (RGSs), GammaART-6000™, and its Chinese equivalents, such as OUR and MASEP, etc., are new radiosurgery systems that use rotating ^{60}Co sources instead of the 201 static sources (Leksell gamma knife, LGK). The rotating sources of RGSs simulate an infinite number of beams and promote extremely high target to surface dose ratios. However, the results of Monte Carlo in this study shows that RGS variants (modeled as having the same latitude angles, source to focus distance, and the distance from the source to the end of the collimator as the LGK) have smaller beam profile penumbra in the z direction, while LGK has smaller penumbra in the x and y directions. The differences are more significant in using larger collimators. © *2006 American Association of Physicists in Medicine*. [DOI: 10.1118/1.2207313]

Key words: gamma knife, stereotactic radiosurgery, Monte Carlo simulation

INTRODUCTION

In 1968, the Swedish neurosurgeon Lars Leksell and the physicist Borje Larsson developed a dedicated radiosurgical tool known as the "gamma knife." The gamma knife is manufactured by Elekta Instruments Inc., a Swedish company which manufactures stereotactic surgery and radiosurgery equipment, based on the inventions of Lars Leksell. The Leksell gamma knife is a radiosurgical tool used to treat deep-seated intracranial tissues, benign or malignant tumours, which are inaccessible or unsuitable for conventional invasive surgery. The gamma knife delivers a single high dose of ionizing radiation, relative to those absorbed by the surrounding normal brain tissues, which is a resultant of 201 static ^{60}Co sources. Each individual beam is mechanically focused through the collimating system onto the target. The Leksell Gamma Knife consists of a radiation unit, individual collimator helmets, and a movable patient couch. Different beam diameters, 4, 8, 14, and 18 mm, can be chosen by the exchange of collimator helmets. This allows lesions of different sizes and shapes to be treated.

There are different generations of the Leksell Gamma Knife unit, such as model-U, model-B, and the latest model-C version. Model U has similar source geometry and dimensions as models B and C, except that model U has larger latitude angles. The disadvantage of model U is that some sources at the superior part of the patient are usually plugged in order to protect the optic chiasm. Models B and C are improved versions by introducing smaller latitude angles. Model C has exactly the same radiation unit as model B. The motorized Automatic Positioning System™ (APS) is the main addition to model C. The APS makes it possible to avoid the manual positioning and repositioning of the stereotactic coordinates during treatments, so shorter treatment time and better selectivity can be achieved for multiple shots strategy.

The rotating gamma systems (RGSs) GammaART-6000™ and its Chinese equivalents, such as (OUR) and (MASEP),[1–7] etc., are new radiosurgery systems that use rotating ^{60}Co sources instead of the 201 static sources [Leksell gamma knife (LGK)]. The operating principle of the RGSs is similar to the LGK.[8–11] For example, the GammaART-6000™ system uses 30 ^{60}Co sources distributed symmetrically around a hemisphere between latitude angles of 13 to 43 deg as measured from the sagittal plane. These sources within the single housing helmet rotate at a speed of approximately 2 to 4 rotations per minute. Inside the source hemisphere, a concentric collimating hemisphere is corotating with the sources, exposing the desired beam diameter such as 4, 8, 14, and 18 mm. Therefore only 30 sources yield a similar treatment technique to the LGK and lower the cost in capital investment and operation expense. Furthermore, the rotating sources of RGS simulate an infinite number of beams and promote extremely high target to surface dose ratios. In this paper, we applied the Monte Carlo technique to simulation models of LGK (model B or C) and RGS. Comparisons on dose profiles along the three principal x, y, and z axes were made between the LGK and the simulation model of LGK with rotating sources.

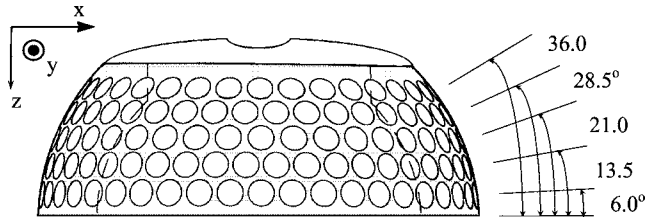

FIG. 1. The Leksell collimator helmet of models B or C showing latitude angles from 6° to 36°.

TABLE I. Coordinates of the 201 static ^{60}Co sources of the LGK with the unit center point at origin and SFD=400 mm.

Source address	X (cm)	Y (cm)	Z (cm)
A1	−2.66	−39.69	−4.18
A2	−7.95	−38.98	−4.18
A3	−13.09	−37.57	−4.18
A4	−17.99	−35.48	−4.18
A5	−22.57	−32.76	−4.18
A6	−26.75	−29.45	−4.18
A8	−32.76	−22.57	−4.18
A9	−35.48	−17.99	−4.18
A10	−37.57	−13.09	−4.18
A11	−38.98	−7.95	−4.18
A12	−39.69	−2.66	−4.18
A13	−39.69	2.66	−4.18
A14	−38.98	7.95	−4.18
A15	−37.57	13.09	−4.18
A16	−35.48	17.99	−4.18
A17	−32.76	22.57	−4.18
A19	−26.75	29.45	−4.18
A20	−22.57	32.76	−4.18
A21	−17.99	35.48	−4.18
A22	−13.09	37.57	−4.18
A23	−7.95	38.98	−4.18
A24	−2.66	39.69	−4.18
A25	2.66	39.69	−4.18
A26	7.95	38.98	−4.18
A27	13.09	37.57	−4.18
A28	17.99	35.48	−4.18
A29	22.57	32.76	−4.18
A30	26.75	29.45	−4.18
A32	32.76	22.57	−4.18
A33	35.48	17.99	−4.18
A34	37.57	13.09	−4.18
A35	38.98	7.95	−4.18
A36	39.69	2.66	−4.18
A37	39.69	−2.66	−4.18
A38	38.98	−7.95	−4.18
A39	37.57	−13.09	−4.18
A40	35.48	−17.99	−4.18
A41	32.76	−22.57	−4.18
A43	26.75	−29.45	−4.18
A44	22.57	−32.76	−4.18
A45	17.99	−35.48	−4.18
A46	13.09	−37.57	−4.18
A47	7.95	−38.98	−4.18
A48	2.66	−39.69	−4.18
B1	−2.71	−38.80	−9.34
B2	−8.09	−38.04	−9.34
B3	−13.30	−36.55	−9.34
B4	−18.26	−34.34	−9.34
B5	−22.86	−31.47	−9.34
B6	−27.02	−27.98	−9.34
B8	−33.68	−19.45	−9.34
B9	−36.06	−14.57	−9.34
B10	−37.74	−9.41	−9.34
B11	−38.68	−4.07	−9.34
B12	−38.87	1.36	−9.34
B13	−38.30	6.75	−9.34
B14	−36.99	12.02	−9.34
B15	−34.96	17.05	−9.34
B16	−32.25	21.75	−9.34
B17	−28.90	26.03	−9.34
B18	−25.00	29.80	−9.34
B19	−20.61	32.98	−9.34
B20	−15.82	35.53	−9.34
B21	−10.72	37.39	−9.34
B22	−5.41	38.52	−9.34
B23	0.00	38.89	−9.34
B24	5.41	38.52	−9.34
B25	10.72	37.39	−9.34
B26	15.82	35.53	−9.34
B27	20.61	32.98	−9.34
B28	25.00	29.80	−9.34
B29	28.90	26.03	−9.34
B30	32.25	21.75	−9.34
B31	34.96	17.05	−9.34
B32	36.99	12.02	−9.34
B33	38.30	6.75	−9.34
B34	38.87	1.36	−9.34
B35	38.68	−4.07	−9.34
B36	37.74	−9.41	−9.34
B37	36.06	−14.57	−9.34
B38	33.68	−19.45	−9.34
B39	30.65	−23.95	−9.34
B40	27.02	−27.98	−9.34
B41	22.86	−31.47	−9.34
B42	18.26	−34.34	−9.34
B43	13.30	−36.55	−9.34
B44	8.09	−38.04	−9.34
B45	2.71	−38.80	−9.34
C1	−5.84	−36.88	−14.33
C2	−11.54	−35.52	−14.33
C3	−16.95	−33.27	−14.33
C4	−21.95	−30.21	−14.33
C5	−26.41	−26.41	−14.33
C7	−33.27	−16.95	−14.33
C8	−35.52	−11.54	−14.33
C9	−36.88	−5.84	−14.33
C10	−37.34	0.00	−14.33
C11	−36.88	5.84	−14.33
C12	−35.52	11.54	−14.33
C13	−33.27	16.95	−14.33
C14	−30.21	21.95	−14.33
C15	−26.41	26.41	−14.33
C16	−21.95	30.21	−14.33
C17	−16.95	33.27	−14.33
C18	−11.54	35.52	−14.33
C19	−5.84	36.88	−14.33
C20	0.00	37.34	−14.33
C21	5.84	36.88	−14.33
C22	11.54	35.52	−14.33
C23	16.95	33.27	−14.33
C24	21.95	30.21	−14.33
C25	26.41	26.41	−14.33
C26	30.21	21.95	−14.33
C27	33.27	16.95	−14.33
C28	35.52	11.54	−14.33
C29	36.88	5.84	−14.33
C30	37.34	0.00	−14.33

TABLE I. (*Continued.*)

Source address	*X* (cm)	*Y* (cm)	*Z* (cm)
C31	36.88	−5.84	−14.33
C32	35.52	−11.54	−14.33
C33	33.27	−16.95	−14.33
C34	30.21	−21.95	−14.33
C35	26.41	−26.41	−14.33
C36	21.95	−30.21	−14.33
C37	16.95	−33.27	−14.33
C38	11.54	−35.52	−14.33
C39	5.84	−36.88	−14.33
C40	0.00	−37.34	−14.33
D1	−2.76	−35.04	−19.09
D2	−8.21	−34.18	−19.09
D3	−13.45	−32.48	−19.09
D4	−18.37	−29.97	−19.09
D5	−22.83	−26.73	−19.09
D7	−29.97	−18.37	−19.09
D8	−32.48	−13.45	−19.09
D9	−34.18	−8.21	−19.09
D10	−35.04	−2.76	−19.09
D11	−35.04	2.76	−19.09
D12	−34.18	8.21	−19.09
D13	−32.48	13.45	−19.09
D14	−29.97	18.37	−19.09
D15	−26.73	22.83	−19.09
D16	−22.83	26.73	−19.09
D17	−18.37	29.97	−19.09
D18	−13.45	32.48	−19.09
D19	−8.21	34.18	−19.09
D20	−2.76	35.04	−19.09
D21	2.76	35.04	−19.09
D22	8.21	34.18	−19.09
D23	13.45	32.48	−19.09
D24	18.37	29.97	−19.09
D25	22.83	26.73	−19.09
D26	26.73	22.83	−19.09
D27	29.97	18.37	−19.09
D28	32.48	13.45	−19.09
D29	34.18	8.21	−19.09
D30	35.04	2.76	−19.09
D31	35.04	−2.76	−19.09
D32	34.18	−8.21	−19.09
D33	32.48	−13.45	−19.09
D34	29.97	−18.37	−19.09
D35	26.73	−22.83	−19.09
D36	22.83	−26.73	−19.09
D37	18.37	−29.97	−19.09
D38	13.45	−32.48	−19.09
D39	8.21	−34.18	−19.09
D40	2.76	−35.04	−19.09
E1	−5.62	−31.87	−23.51
E2	−11.07	−30.41	−23.51
E3	−16.18	−28.03	−23.51
E4	−20.80	−24.79	−23.51
E6	−28.03	−16.18	−23.51
E7	−30.41	−11.07	−23.51
E8	−31.87	−5.62	−23.51
E9	−32.36	0.00	−23.51
E10	−31.87	5.62	−23.51
E11	−30.41	11.07	−23.51
E12	−28.03	16.18	−23.51
E13	−24.79	20.80	−23.51
E14	−20.80	24.79	−23.51
E15	−16.18	28.03	−23.51
E16	−11.07	30.41	−23.51
E17	−5.62	31.87	−23.51
E18	0.00	32.36	−23.51
E19	5.62	31.87	−23.51
E20	11.07	30.41	−23.51
E21	16.18	28.03	−23.51
E22	20.80	24.79	−23.51
E23	24.79	20.80	−23.51
E24	28.03	16.18	−23.51
E25	30.41	11.07	−23.51
E26	31.87	5.62	−23.51
E27	32.36	0.00	−23.51
E28	31.87	−5.62	−23.51
E29	30.41	−11.07	−23.51
E30	28.03	−16.18	−23.51
E31	24.79	−20.80	−23.51
E32	20.80	−24.79	−23.51
E33	16.18	−28.03	−23.51
E34	11.07	−30.41	−23.51
E35	5.62	−31.87	−23.51
E36	0.00	−32.36	−23.51

METHODS AND MATERIALS

The Monte Carlo system employed was the PRESTA (parameter reduced electron-step transport algorithm) version of the EGS4 (electron gamma shower) computer code. Detailed descriptions on the structure of the EGS4 code can be found in Jenkins *et al.*[12]

In the simulation of LGK (model B or C) with static sources, the patient's head was modeled by a spherical water phantom, with a diameter of 160 mm. Each one of the 201 sources located in the radiation unit is composed of 20 ^{60}Co pellets 1 mm in diameter and 1 mm in length. Each source was therefore modeled by a cylinder 1 mm in diameter and 20 mm in length. The ^{60}Co sources are arranged in a sector of a hemispherical surface with a radius of about 400 mm. They are distributed along five parallel circles separated from each other by an angle of 7.5° (6.0°, 13.5°, 21.0°, 28.5°, 36.0°) as shown in Fig. 1. Table I shows the coordinates of the 201 ^{60}Co sources with the source to focus distance (SFD)

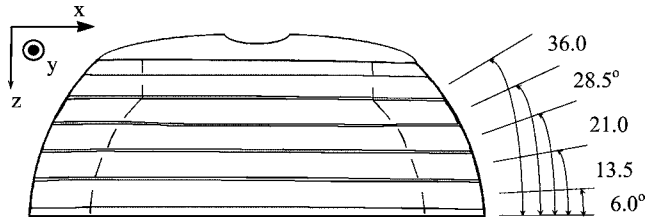

FIG. 2. The rotating sources simulating an infinite number of beams and each beam pointing at the unit center point (100, 100, 100).

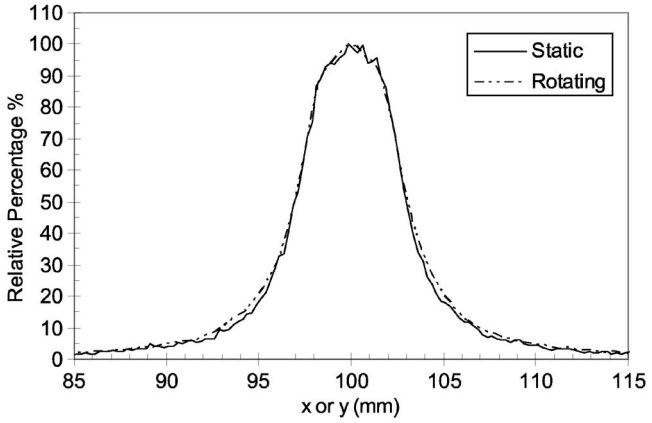

FIG. 3. Comparisons of the dose profiles along the x or y axis of the 4 mm collimator helmet between the cases using 201 static sources and rotating sources.

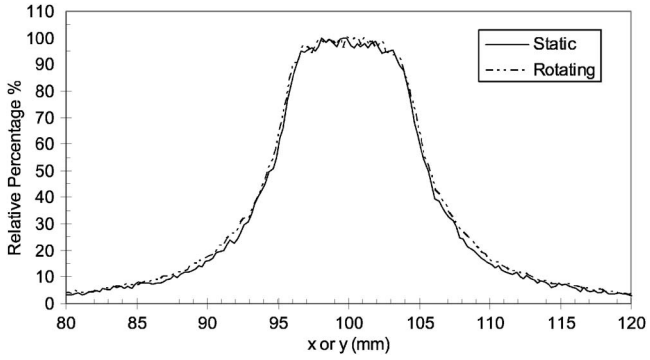

FIG. 5. Comparisons of the dose profiles along the z axis of the 4 mm collimator helmet between the cases using 201 static sources and rotating sources.

of 400 mm. The unit center point (100, 100, 100) was offset to the origin. The 201 radiation beams coming from the 201 static sources pass through the opening of the collimators to the target point. The diameters of the radiation beams at the focus are defined by the size of the collimator apertures. A single shot was delivered at the unit center point (100, 100, 100) of the phantom. For the 14 and 18 mm collimator helmets, scoring bins with dimensions 0.5 mm $\times$ 1 mm $\times$ 1 mm were defined along the x, y, and z axes. For the 4 and 8 mm collimator helmets, the dimensions of the scoring bins were 0.25 mm $\times$ 0.5 mm $\times$ 0.5 mm. The dimensions of scoring bins were small enough to give a high resolution of the dose profiles and were large enough to give good statistical results. Histories of 3.0×10^7 were performed for the 4 and 8 mm collimator helmets, and histories of 6.2×10^7 were performed for the 14 and 18 mm collimator helmets. All history runs were divided into 20 batches for calculation of statistics and were large enough to give a standard error of about 4% at the dose maximum region. The standard error in the lower isodose regions will be much smaller because of the creation of many secondary particles farther downstream. The photon spectrum of ^{60}Co was taken from Amersham,[13] which consisted of two peaks at 1.173 and 1.333 MeV. The cut-off energies for electrons and photons were set to be 0.521 MeV (rest mass of electron + 0.01 MeV) and 0.01 MeV, respectively. High cut-off energies shortened the simulation time at the expense of reliable results. In our study, further lowering these cut-off energies caused no observable differences of the output results.

In the simulation of LGK with rotating sources, the whole setup and parameters were the same except the source distribution. Five circular cone-shaped radiation fields were used to simulate the rotating sources as shown in Fig. 2. The SFD was kept at 400 mm which was the same as that in LGK. Shortening the SFD or the distance from the source to the end of the collimator would certainly worsen the geometric penumbra. The same history runs (same primary photons) were used in order to obtain the same absolute maximum dose.

RESULTS AND DISCUSSION

Figures 3 and 4 show the comparison of the dose profiles along the x or y axis of the 4 and 8 mm collimator helmets, respectively, between the cases using 201 static sources and rotating sources. The gamma knife system using static sources has a better beam profile penumbra than the gamma knife systems using rotating sources in the x or y direction. The reason is that the scattered radiation increases along the x or y direction in the beam profile as the number of beams using rotating sources increase mainly in the x or y direction.

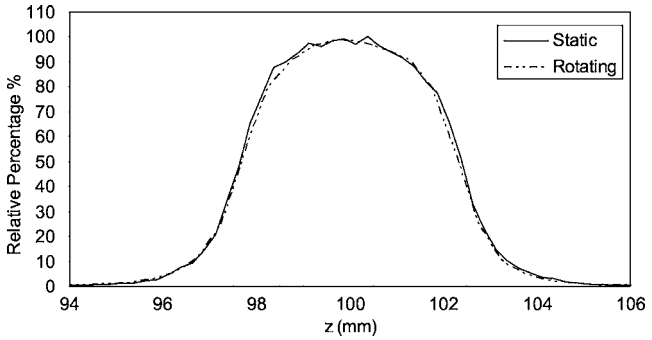

FIG. 4. Comparisons of the dose profiles along the x or y axis of the 8 mm collimator helmet between the cases using 201 static sources and rotating sources.

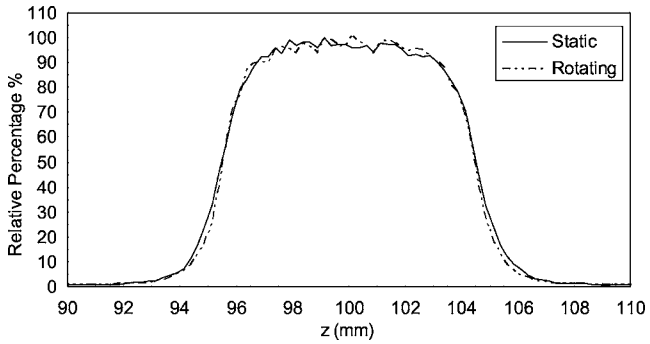

FIG. 6. Comparisons of the dose profiles along the z axis of the 8 mm collimator helmet between the cases using 201 static sources and rotating sources.

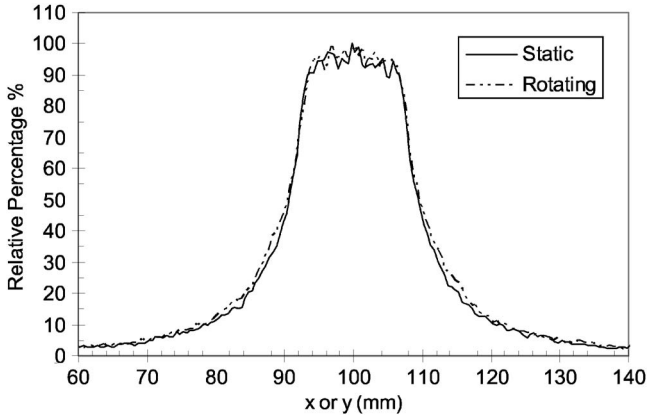

FIG. 7. Comparisons of th dose profiles along the x or y axis of the 14 mm collimator helmet between the cases using 201 static sources and rotating sources.

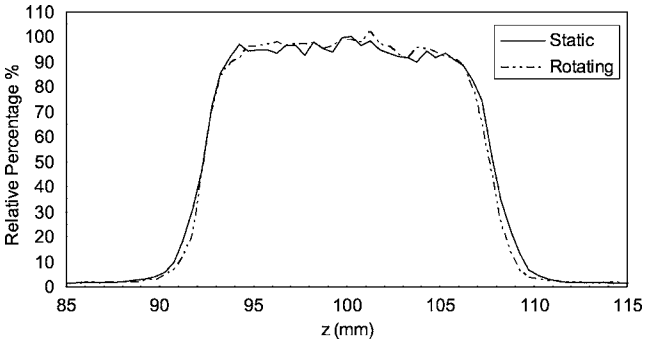

FIG. 8. Comparisons of the dose profiles along the z axis of the 14 mm collimator helmet between the cases using 201 static sources and rotating sources.

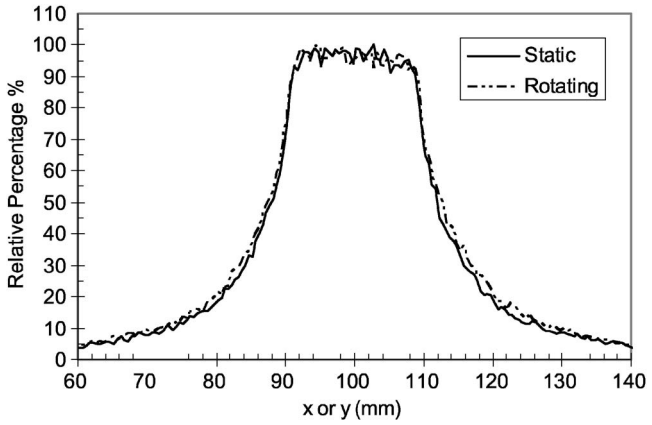

FIG. 9. Comparisons of the dose profiles along the x or y axis of the 18 mm collimator helmet between the cases using 201 static sources and rotating sources.

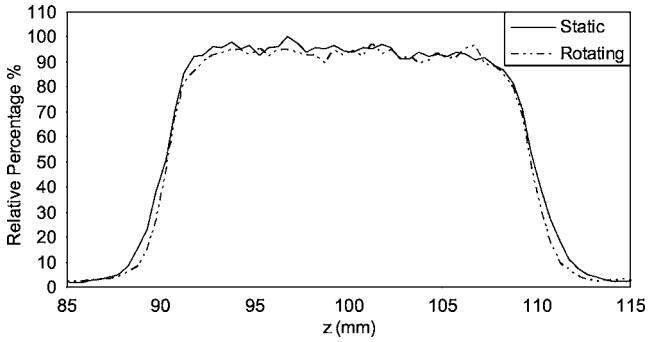

FIG. 10. Comparisons of the dose profiles along the z axis of the 18 mm collimator helmet between the cases using 201 static sources and rotating sources.

TABLE II. Comparison of the widths at 50% level (FWHM) between the cases using static and rotating sources.

Collimator-Direction	FWHM (static) (mm)	FWHM (rotating) (mm)
4 mm-x or y	6.0	6.1
4 mm-z	4.8	4.6
8 mm-x or y	11.1	11.5
8 mm-z	9.1	9.0
14 mm-x or y	18.8	19.5
14 mm-z	15.6	15.3
18 mm-x or y	24.0	25.4
18 mm-z	19.7	19.4

Figures 5 and 6 show the comparison of the dose profiles along the z axis of the 4 and 8 mm collimator helmets, respectively, between the cases using 201 static sources and rotating sources. The gamma knife systems using rotating sources have a better beam profile penumbra than the gamma knife system using static sources in the z direction. The differences are even more significant for larger collimator helmets, e.g., the 14 and 18 mm collimator helmets, as shown in Figs. 7–10. The reason is that the larger collimators will generate more scattered radiation. Tables II and III show the comparison of the profile penumbra between the cases using static and rotating sources. Table II shows the widths at 50% levels (full width half maximum, FWHM) while Table III shows the widths at 20% levels. In lower-percentage regions, scattered secondary particles are more abundant, so the differences are more significant.

In addition, some RGSs use ^{60}Co sources which are distributed symmetrically around a hemisphere using larger latitude angles, for example 13° to 43° (Ref. 2) and 15° to 52°.[3] In comparison, the LGK models B and model C use 6° to 36° as shown in Fig. 1. Theoretically, using larger latitude angles will improve the beam profile penumbra a bit. Larger latitude angles mean larger solid angles. The beams converge from larger solid angles lead to smaller radiation doses delivered to normal healthy tissues surrounding the target, because the dose to the normal tissue is spread over a larger volume.

TABLE III. Comparison of the widths at 20% level between the cases using static and rotating sources.

Collimator-Direction	Width at 20% level (static) (mm)	Width at 20% level (rotating) (mm)
4 mm-x or y	9.5	10.2
4 mm-z	5.9	5.9
8 mm-x or y	17.9	18.7
8 mm-z	10.6	10.2
14 mm-x or y	30.3	31.9
14 mm-z	17.6	16.9
18 mm-x or y	39.2	41.2
18 mm-z	22.2	21.2

However, using larger latitude angles will increase the absorbed dose along the z direction. The situation is similar to the old model U of Leksell Gamma Knife.[14]

[a]Electronic mail: appetery@cityu.edu.hk

[1]*American Radiosurgery Inc., Next-Generation in Radiosurgery Technology, Medco Forum®*, Vol. 12, No. 12 (Medco Communications, Evergreen, CO, 2005).
[2]S. J. Goetsch, B. D. Murphy, R. Schmidt, J. Micka, L. De Werd, Y. Chen, and S. Shockley, "Physics of rotating gamma systems for stereotactic radiosurgery," Int. J. Radiat. Oncol., Biol., Phys. **43**, 689–696 (1999).
[3]H. D. Kubo and F. Araki, "Dosimetry and mechanical accuracy of the first rotating gamma system installed in North America," Med. Phys. **29**, 2497–2505 (2002).
[4]A. H. Maitz and A. Wu, "Treatment planning of stereotactic convergent gamma-ray irradiation using Co-60 sources," Med. Dosim **23**, 169–175 (1998).
[5]H. K. Raouf, "Gamma knife and linear accelerator stereotactic radiosurgery," Agence d'évaluation des technologies et des modes d'intervention en santé (AETMIS), (AETMIS 02–03). Montréal AETMIS, 2004, p. xvii-76.
[6]H. Wang and J. Luo, "Rotating gamma stereotactic radiosurgery system," Zhongguo Yi Liao Qi Xie Za Zhi **22**, 272–274 (1998).
[7]D. Zhou, Z. Liu, X. Yu, S. Qi, and J. Du, "Rotating gamma system radiosurgery for cerebral arteriovenous malformations," Stereotact Funct Neurosurg. **75**, 109–116 (2000).
[8]*Leksell Gamma Unit-User's Manual* (Elekta, Geneva, Switzerland), Vol. 1.
[9]*Leksell GammaPlan Instructions for Use for Version 4.0-Target Series* (Elekta, Geneva, Switzerland, 1991).
[10]A. Wu, "Physics and dosimetry of the Gamma Knife," Neurosurg. Clin. N. Am. **3**, 35–50 (1992).
[11]A. Wu, G. Lindner, A. H. Maitz, A. M. Kalend, L. D. Lunsford, J. C. Flickinger, and W. D. Bloomer, "Physics of gamma knife approach on convergent beams in stereotactic radiosurgery," Int. J. Radiat. Oncol., Biol., Phys. **18**, 941–950 (1990).
[12]M. Jenkins, W. R. Nelson, and A. Rindi, *Monte Carlo Transport of Electrons and Photons* (Plenum, New York, 1988).
[13]*Medical Radiation Sources Catalogue* (Amersham, Buckinghamshire, England, 1982).
[14]J. S. Kuo, C. Yu, S. L. Giannotta, Z. Petrovich, and M. L. Apuzzo, "The Leksell gamma knife Model U. versus Model C: A quantitative comparison of radiosurgical treatment parameters," Neurosurgery **55**, 168–172 (2004); **55**, 172–173 (2004).